Available online at www.sciencedirect.com
SCIENCE DIRECT®
PERGAMON
International Journal of Heat and Mass Transfer 46 (2003) 1155–1169
International Journal of HEAT and MASS TRANSFER
www.elsevier.com/locate/ijhmt

Inverse influence of initial diameter on droplet burning rate in cold and hot ambiences: a thermal action of flame in balance with heat loss

Guangwen Xu [a], Masiki Ikegami [a,*], Senji Honma [a], Kouji Ikeda [a], Xiaoxun Ma [a], Hiroshi Nagaishi [a], Daniel L. Dietrich [b], Peter M. Struk [c]

[a] National Institute of Advanced Industrial Science and Technology (AIST), Sapporo 062-8517, Japan
[b] NASA Glenn Research Center, Mail Stop 110-3, 21000 Brookpark Road, Cleveland, OH 44135, USA
[c] National Center for Microgravity Research, Cleveland, OH 44135, USA

Received 5 March 2002; received in revised form 20 September 2002

Abstract

Isolated droplet burning were conducted in microgravity ambiences of different temperatures to test the initial diameter influence on droplet burning rate that shows a flame scale effect and represents an overall thermal action of flame in balance with heat loss. The coldest ambience examined was room air, which utilized a heater wire to ignite the droplet. All other ambiences hotter than 633 K were acquired through an electrically heated air chamber in a stainless steel can. An inverse influence of initial droplet diameter on burning rate was demonstrated for the cold and hot ambiences. That is, the burning rate respectively decreased and increased in the former and latter cases with raising the initial droplet diameter. The reversion between the two influences appeared gradual. In the hot ambiences the burning rate increase with increasing the initial droplet diameter was larger at higher temperatures. A "net heat" of flame that denotes the difference between "heat gain" by the droplet and "heat loss" to the flame surrounding was suggested responsible for the results. In low-temperature ambiences there is a negative net heat, and it turns gradually positive as the ambience temperature gets higher and the heat loss becomes less. Relating to luminous flame sizes and soot generation of differently sized droplets clarified that the flame radiation, both non-luminous and luminous, is determinative to the net heat in microgravity conditions. In addition, the work identified two peak values of soot generation during burning, which appeared respectively at the room temperature and at about 1000 K. The increase in ambience temperature made also bigger soot shells. The heat contribution of flame by both radiation and conduction was demonstrated hardly over 40% in the total heat required for droplet vaporization during burning in a hot ambience of 773 K.

Keywords: Microgravity combustion; Droplet combustion; Flame radiation; Soot; Initial diameter influence

1. Introduction

For isolated droplet burning, the heat that gains from flame via conduction, radiation and convection positively works on, even decides the burning rate [1,2]. Meanwhile, the heat exchange occurs also between the flame and its surrounding, which makes a "heat loss" for the flame (such as the radiative heat loss so far extensively analyzed [3–5]). Therefore, there is a "net heat" that denotes the difference between the "heat gain" by the droplet and heat loss to the ambience. This net heat determines an overall action of flame on burning, its understanding is thus important to combustion problems. For a given flame, it may be difficult to identify the net heat unless the heat gain and heat loss are both

* Corresponding author. Tel.: +81-11-857-8961; fax: +81-11-857-8900.
E-mail address: m.ikegami@aist.go.jp (M. Ikegami).

0017-9310/03/$ - see front matter
PII: S0017-9310(02)00397-6

known. The net heat, however, possesses an important characteristic of proportionally varying with flame scale, making it possible to analyze the net heat through investigating the flame scale influence. For example, a zero net heat must lead to a zero influence of flame scale, while a negative net heat would cause the burning rate to decrease with increasing the flame scale. The latter just corresponds to the recent examinations of initial diameter influences on droplet burning rate [6–13] and extinction droplet diameter [10–13] in microgravity ambiences at room temperature, where varying the initial droplet diameter changed actually the flame scale.

With *n*-heptane and 1-chloropentane droplets, Jackson et al. [6,7] first observed that the burning rate in ambient air gradually decreased with increasing the initial diameter d_0. This was then verified by microgravity burning tests using either drop towers [8,9] or spacelabs [10–13], even in alternative ambiences that had different pressures, oxygen fractions and dilution gases (nitrogen or helium) [11,12]. The tested fuels for those examinations were various, mainly including *n*-heptane [8,11,12], nonane [9], methanol/water [10] and ethanol/water [13]. So far, the lower burning rate for larger droplet in microgravity room ambiences was suggested mainly relative to the radiant heat loss from the flame, which is higher for larger droplet [8–15]. Reflecting to the net heat concept shown above, this indicates a gradually increased negative net heat of flame radiation as the diameter d_0 was raised. While the luminous radiation via soot particles was generally considered [8–12], Dryer et al. [13], with evidences of model prediction [14,15], stressed a major contribution by non-luminous radiation of burning gases. The real fact may be that both the types of flame radiation are similarly important, as recently demonstrated by Manzello et al. [16] through modeling. For less-sooting flames, such as of methanol/water [10,14], however, the non-luminous radiation should be dominant.

At a specified burning time relative to d_0 squared, i.e. $(t - t_d)/d_0^2$, an initially larger droplet possesses a larger flame diameter [8,11], which causes a higher non-luminous radiation and in turn a greater negative net heat (here t_d referring to ignition delay). The larger droplet has also a higher soot yield that shows as a higher local soot density (volume fraction) at soot shell [6,7,17] and a greater total soot amount across the flame [8] at a given burning time $(t - t_d)/d_0^2$ (even in hot ambience [18]). This in turn increases the luminosity of the flame of an initially larger droplet and produces a higher luminous radiation to enlarge the negative net heat. The higher soot amount inside the flame (a denser soot shell) may influence the burning also by acting as a heat sink or a heat/mass transfer barrier [6,7]. The recent analyses of Lee et al. [8] and Manzello et al. [16], however, clarified that the action of luminous radiation would be more profound than the others.

Different influences were also reported for the initial diameter on droplet burning rate in microgravity room ambiences. The earliest microgravity tests of Kumagai and co-workers [19–21] identified a slight increase of burning rate with increasing d_0. Later, Choi et al. [22] and Hara and Kumagai [23] showed that the burning rate is almost independent of d_0, although the enhanced soot formation for larger droplets was similarly identified [23]. Very little variation of burning rate with d_0 was also observed by Suekane et al. [24] for droplets in convective flows. Manzello et al. [16] recently found that increasing the initial diameter d_0 first decreased, and then inversely increased the burning rate when d_0 become certainly larger. The excessively higher non-luminous radiation for such bigger droplet was suggested responsible for this inverse increase. That is, the radiation-induced negative net heat may increase to such a value that cools the flame to an extent whereat the fuel vapor pyrolysis becomes impossible. This produces then less soot [11,25], shown as a blue flame in appearance, and reduces the negative net heat of luminous radiation. As a consequence, there displays a local increase in burning rate, despite the rate itself is yet lower than those of much smaller droplets [16]. Notwithstanding, all burning rate constants k measured by Williams [12] and Dryer et al. [13] from spacelabs did not show any inverse increase, even when d_0 was up to 6.0 mm. In atmospheric helium-oxygen ambience, Nayagam et al. [11] observed that the dependence of burning rate on d_0 varied with the oxygen fraction in the ambience. While the sooting flame in the highest oxygen ambience of 35 vol.% decreased the burning rate of initially larger droplet, the other less-sooting flames in oxygen-reduced ambiences little varied (O_2: 30 vol.%) or inversely increased (O_2: 25 vol.%) the burning rate with raising d_0. The reason for these different dependences, however, was not clearly stated by those authors.

For microgravity droplet burning in cold ambience, another important phenomenon related to the negative net heat is the flame extinction before fuel burnout. When flame is definitely larger, the negative net heat (heat loss) may become excessively high, which cools the flame to such a temperature that is lower than the values required by burning reactions. This causes then flame extinction, even though there is still some fuel, shown as the extinction droplet diameter, left in the droplet. The phenomenon was theoretically predicted by Chao et al. [3] through an asymptotic analysis considering radiative heat loss, and was experimentally observed by many microgravity droplet burning tests in room ambiences [10–13,25,26]. An important result obtained is that the extinction droplet diameter increases as increasing the initial droplet diameter for a given fuel burnt in a specified ambience. Marchese et al. [15,16] recently reproduced this result by a modelling that accounts for

non-luminous radiation, showing that it is the higher heat loss (negative net heat) of a larger droplet that gives a greater extinction droplet diameter. When burning methanol droplets, the water absorption by the droplet from burning gases was also employed to reason the increase of extinction droplet diameter with increasing d_0 [27]; this obviously is hardly applicable to other fuels like alkanes. The extinction droplet diameter was also larger in oxygen-helium ambience than in air [26]. The higher heat conductivity of helium than nitrogen was suggested responsible for the result. That is, there is higher heat conduction from flame to ambience in this case, which results in a higher negative net heat and the easier flame extinction accordingly.

Therefore, it is the net heat, shown as a heat loss in room ambiences, of the flame that determines the initial diameter influences on droplet burning rate and extinction droplet diameter. The net heat, on the other hand, is fully decided by radiation and conduction in microgravity, it is thus closely dependent on the ambience temperature. An intuition is that as the temperature increases, the heat transfer between the flame and ambience decreases, whereas that between the flame and droplet inversely increases. This is a result controlled by the increased flame temperature but little varied droplet temperature (droplet temperature being subject to the fuel boiling point). Consequently, the negative net heat prevailing in room ambiences must gradually descend and finally reverse to positive with increasing the ambience temperature. For that, there must exist some different initial diameter influences on the droplet burning rate and extinction droplet diameter.

When the above concern appears plausible, we noted that the tests so far conducted were nearly all in room ambiences. This leads to the present work that makes the first extension of such studies to a high-temperature ambience (air) to show how the net heat changes with the ambience temperature. For that, the influence of initial diameter on droplet burning rate is examined in airs with different temperatures. Microgravity is employed to exclude the gravity-induced convections. There were very few reports about droplet burning in microgravity hot ambiences, except for an early study of Faeth and Olson [28] on ignition and a recent observation of Xu et al. [18] on sooting. This work will analyze the droplet burning and vaporization rates in microgravity hot conditions.

2. Experimental

The experiments involved two different apparatuses. As detailed below, the apparatus I in Fig. 1 using a wire heater as the igniter was employed to implement the droplet burning in room ambience (air), while the apparatus II in Fig. 2 with a hot-air chamber was adopted

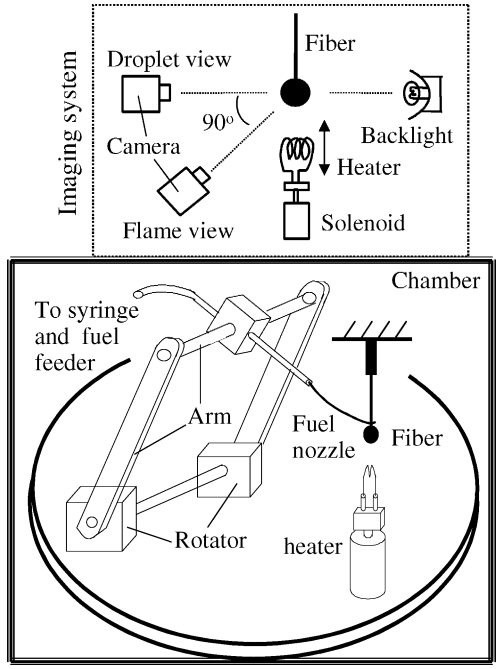

Fig. 1. A diagram of apparatus I using a heater igniter.

to burn and vaporize droplets in atmospheric hot airs. Microgravity conditions were generated through the drop tower in either the Japan Microgravity Center (JAMIC, 10-s) or the NASA Glenn Research Center (2.2-s).

2.1. Apparatus I using a heater igniter

Fig. 1 is a schematic diagram of the apparatus I, with an up-sided box illustrating the image system. The igniter was an aluminum–kanthal alloy wire that had a

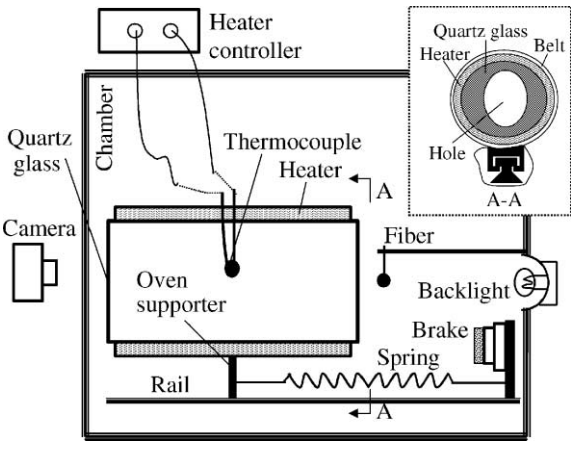

Fig. 2. A diagram of apparatus II using a hot chamber.

resistance of approximately 1.2 Ω. A DC motor-activated syringe created the fuel droplet. The motor rotated an arm, which in turn carried a fuel nozzle to move towards or away from a quartz fiber. The fuel nozzle was fixed on the arm and was connected to a micro syringe that was moved by a feeder pump. Normally, the nozzle was definitely away from the fiber, and at about 30–40 s before microgravity started (dropping capsule) it was rotated down to a position suitable for fuel transition from the nozzle to the fiber. The feeder pump was then activated to inject a measured amount of fuel into the nozzle that in turn sent the fuel to the fiber. Rotating back of the nozzle caused the droplet to be finally suspended on the fiber bead and to be ready for test. The entire process of droplet creation took usually 20 s, and repetition of the process was allowed. A backlight was turned on at the beginning of the first droplet creation process. Then, microgravity was started, and one second later the igniter was up-moved under the control of a solenoid and turned on for a preset period of time, typically 1.6 s. The actual time, however, usually varied more or less, as to ensure the igniter for an immediate withdrawal after the droplet ignition. The current passing through the igniter was maintained at 3.5 A approximately.

For the apparatus I, image data were taken from two orthogonally located CCD cameras, as indicated in the upside dot line box. This allowed the simultaneous measures of a backlit view for droplet and a direct view for flame. The droplet view provided a measure of droplet size and a demonstration of soot formation during burning, while the flame view enabled a judgment of flame luminosity and a determination of flame sizes. Using this cold-ambience apparatus, only droplet burning was tested.

2.2. Apparatus II using a hot chamber

The hot chamber for apparatus II, as illustrated in Fig. 2, was a ring-pull can that was made of stainless steel and had sizes of 140 mm in length, 70 mm in diameter and 0.5 mm in shell thickness. Two pieces of quartz glasses bottomed the can, with the rear (left) bottom completely closed and the front (right) bottom centrally holed, as small as possible, for the entry of the fiber-tethered droplet. A sheathed heater (Ni–Cr wire) with a heat capacity of about 800 W at 80 V evenly wrapped about the can. The heater was further bound up with heat insulation wools, which made the oven an O.D. of about 100 mm. A chromium–alumel (K-type) thermocouple measured the temperature inside the can, which in turn sent the measured data to a temperature controller. Via a belt, the whole oven was fastened on a support that sat on a railroad and connected with a spring and a rope respectively in the front and rear sides of the oven (rope being not shown in Fig. 2). The other end of the rope was knocked on a rotary solenoid at the far rear (left) and that of the spring was fixed on a stand at the far front (right) side. On the stand there was a brake for oven stop. A quartz fiber suspended the fuel droplet in the oven front, and the droplet was created using a syringe similar as for the apparatus I. There was usually a distance of about 3.5 cm, with a shutter in-between, from oven to fiber. A step motor controlled the shutter to rotate back-to-front or vice versa. In the left side of the oven, a camera was set to view the droplet and the burning. Depending on the fiber orientation that was either vertical or horizontal, either a side (JAMIC) or bottom (NASA) view was possible. Nonetheless, only one image, either of backlit or flame view, was available for a given test from the camera.

Before test, the rope was knocked to pull the oven towards the rear side and to stretch the spring as well. The test was started with heating the oven at usually 3–4 min before the onset of microgravity. Four DC batteries supplied the electricity of heater in NASA, while a slide-transformer adjusted AC was used for that in JAMIC. The typical voltage for the heater was about 80 V, giving a current of about 10 A passing through the heater. Similar as for the apparatus I, the droplet formation proceeded at about 40 s before the microgravity conditions started. At the start of microgravity, the electricity supply for heater was turned off and the shuttle was activated to open. Half a second later (in JAMIC) or just at the capsule drop (in NASA) the rope fastening the oven was un-knocked by the rotary solenoid. This in turn caused the oven to move from rear to front along the railroad, and, as a consequence, to include the fuel droplet into the hot chamber. The movement of the oven took usually 0.12 s till it finally braked (by the brake). The spherical soot shell shown later (Fig. 6) indicates that there was little disturbance to the chamber air during this movement. Via finely adjusting the position of the fiber, the droplet could stop at a location just downright the thermocouple bead. The chamber temperature T_c was varied between 633 and 1123 K to test both droplet burning and vaporization.

2.3. Data reduction and fuel

In all tests, the used quartz fibers had a diameter of 110 μm and a tip bead of 500 μm, and the CCD cameras were connected to digital VCRs. The VCR data were then transferred into a computer using a frame grabber card, giving image (AVI) files that were finally framed at a rate of 60 Hz in the succeeding processes of data reduction.

The droplet size d during burning and vaporization was measured from the backlit views to define the burning and vaporization rate. For this, a time t of burning and vaporization was defined by counting the time from the moment turning on the igniter for the

apparatus I and from the entry of the droplet into the chamber for the apparatus II. The stated droplet size refers generally to an equivalent value that was determined as the cubic root of the product of droplet width squared and droplet length, i.e. $(\text{width})^{2/3} \times (\text{length})^{1/3}$. This equivalent diameter was directly measured for the side view, but indirectly decided from a correlation between the diameter and droplet width for the bottom view (from the bottom view only droplet width being available). The initial droplet diameter d_0 was measured usually at the time of $t = 0$. The sizes of luminous flame (only for apparatus I) and soot shell were also measured respectively from the flame and backlight views. Unlike droplet diameter, the lateral widths of flame and soot shell were adopted to represent their sizes, on account of that the cooling effects of quartz fiber may greatly deform their longitudinal shapes.

The tested fuel in this article was *n*-decane, and the examined d_0 varied between 0.8 and 1.6 mm.

3. Influence identification

Fig. 3 shows the typical curves of droplet size variation during burning and vaporization attained in different ambience temperatures. While the lateral row "a" refers to the burning in room air, rows "b" and "c" show respectively the tests for droplet burning ($T_c = 1093$ K) and vaporization ($T_c = 633$ K) in hot-air ambience. The curves plotted in inset 1 (left) are for d^2 vs. t, while that in inset 2 (right) are about (d/d_0^2) vs. t/d_0^2.

All the size variations in Fig. 3 can be analyzed using the d^2-law [29]. This defines a rate constant k, i.e. the slope of the line in Fig. 3, for the quasi-steady period of burning or vaporization of every individual droplet (k_b for burning, k_v for vaporization). While the curve d^2 vs. t in inset 1 enables a better determination of k, as can be seen from Fig. 3(a1) compared to Fig. 3(a2), the plotting of (d/d_0^2) vs. t/d_0^2 in inset 2 is obviously more distinguishable for the initial diameter influence on k. For example, when one hardly judge an effect of d_0 on burning (Fig. 3(a1)) and vaporization (Fig. 3(c1)) rate from Fig. 3(a1) and (c1), Fig. 3(a2) and (c2) show clearly that k respectively decreased and increased with increasing d_0. A bigger burning rate constant k can be also identified from Fig. 3(b1) for a larger d_0 but the identification is rather distinct in Fig. 3(b2). Further, comparing Fig. 3(b2) and (c2) clarifies that the diameter-induced influence on k is definitely higher in Fig. 3(b2) at higher T_c. Therefore, there existed different relations between k and d_0 for the tests in Fig. 3(a)–(c). Generally, the diameter d_0 exhibited inverse influence on the rate constant k in cold (3a) and hot (3b and 3c) ambiences, and in the hot ambience the influence of d_0 is larger at higher T_c.

For further verification, Fig. 4 summarizes the burning and vaporization rate constants k derived from all the examinations. The data from the JAMIC and NASA drop towers generally consisted with each other. That is, the rate constant had lower values for vaporization (below dot line), and increasing the chamber temperature T_c raised the rate constant both for burning (k_b) and for vaporization (k_v). Nonetheless, comparing the k_b at 973 K from JAMIC (●) with that at 1093 K (△) and 943 K (○) from NASA, also the k_v at 773 K from JAMIC (■) with that at the same T_c from NASA (◇), we may feel that the test in JAMIC had led to somewhat higher values in rate constant. This difference might be relative to many factors that lead to experimental deviations, but the major two factors should be the different microgravity qualities and ovens. Between the NASA and JAMIC tests we in fact changed the oven for once due to a trouble in the apparatus. In addition, one may note that k_v (■) and k_b (□) show simultaneously for $T_c = 773$ K (JAMIC); about this we will provide a further analysis in Fig. 11. For the tests in NASA at 773 K, droplet ignition similarly occurred but was mostly near the end of the microgravity duration.

Nonetheless, all the rate constants k in Fig. 4 exhibited the dependences, which are consistent with Fig. 3, on the initial diameter d_0. That is, the increase in d_0 decreased k in room air (▼) but increased k in the tested hot ambiences, even for vaporization (◆□). Further, the degree increasing k with d_0 is bigger at higher T_c for both burning (above dot line) and vaporization (below dot line). If using a straight line, as illustrated in Fig. 4, to correlate k for every individual T_c with d_0, we can then get a parameter $\delta k/\delta d_0$, the slope of the line, to quantitatively express the magnitude of the initial diameter influence. Fig. 5 correlates the resultant $\delta k/\delta d_0$ from the lines in Fig. 4 with the ambience temperature T_c, where the room temperature was assigned a value of 300 K. For comparison as well as validation, the figure shows also several $\delta k/\delta d_0$ determined from the literature data of k vs. d_0 for burning at room temperature ($d_0 < 1.8$ mm). Based on these data, we can see that the presently measured $\delta k/\delta d_0$ (◆) agree well with the literature reports, especially after the exclusion of the only higher value of Jackson and Avedisian [7].

The magnitude of influence appears uniquely correlative with the ambience temperature, irrespective of the data source that is either from burning or from vaporization. On the whole, the influence, i.e. the value of $\delta k/\delta d_0$, progressively ascended with raising T_c, with a gradual transition from negative ($\delta k/\delta d_0 < 0$) in cold ambience to positive ($\delta k/\delta d_0 > 0$) in hot ambience. The increasing degree of the influence with respect to unit change of T_c, which is $\delta(\delta k/\delta d_0)/\delta T_c$, was also larger at higher T_c, indicating a gradually quicker increase of the initial diameter influence with increasing T_c. The reversion of $\delta k/\delta d_0$ from negative to positive defines a

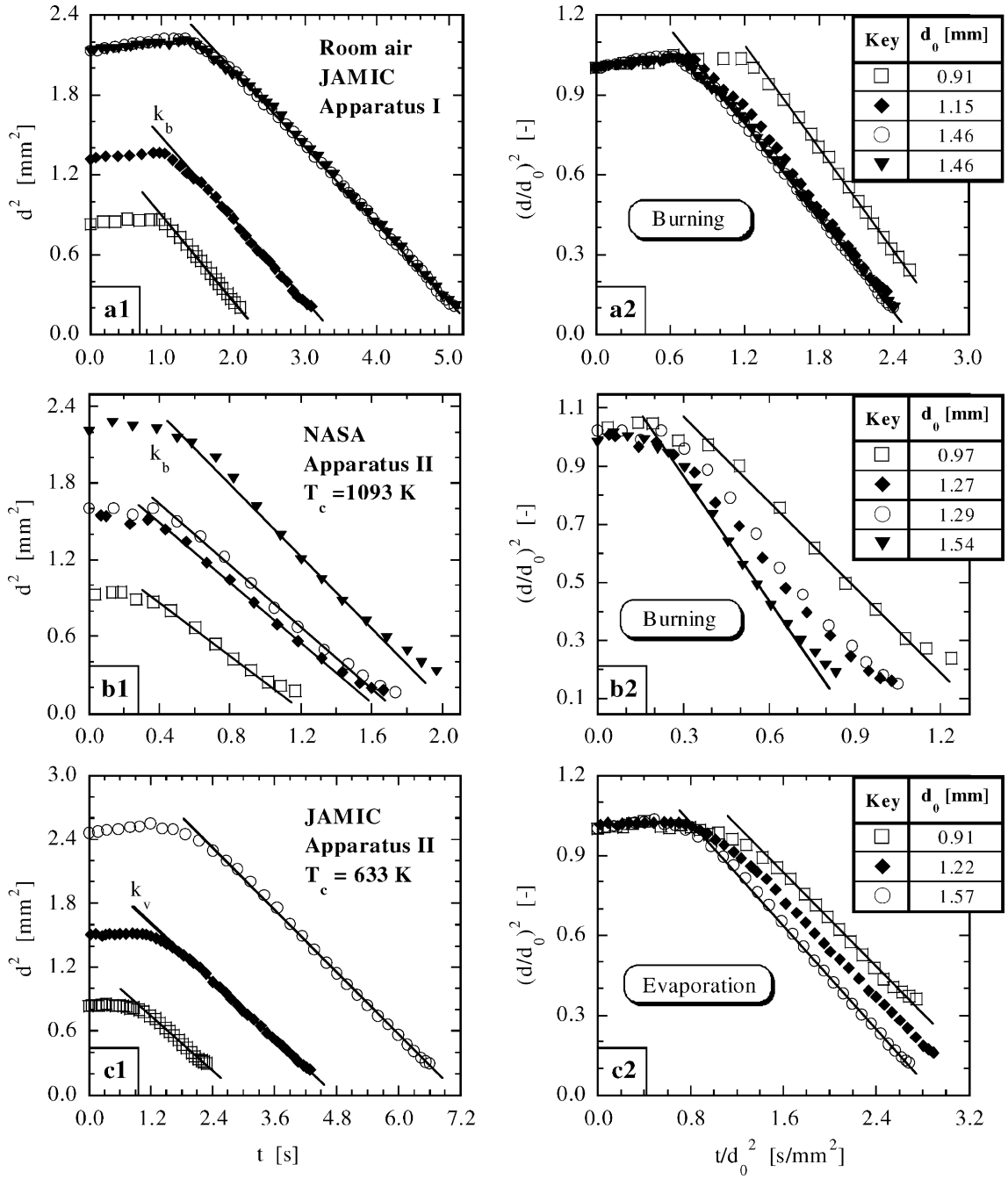

Fig. 3. Typical size variations plotted according to the d^2-law during burning and vaporization in room and hot ambiences.

particular ambience temperature, say, T_{cr}, that may imply some important fundamentals. At least, we believe that it corresponds to a zero net heat, as will be shown further in Section 5.

Figs. 3–5 showed again that the microgravity burning in room ambience possessed an initial diameter influence that decreases the burning rate of larger droplets ($d_0 < 1.8$ mm). On the other hand, the positive influence of d_0 upon burning and vaporization rate in hot-air ambiences was also observed by our tests in normal-gravity conditions for different fuels [30,31]. However, the gravity-induced convection in that case may be also relative to its observed influence, according to the results of Monaghan et al. [32].

Key	T_c [K]	View (Apparatus)	Test case
◇	773	Bottom (II)	Vaporization
○	943		Burning
△	1093		
▼	Room T_c	Side (I)	Burning
◆	633	Side (II)	Vaporization
■	773		
□	773		Burning
●	973		
▲	1123		

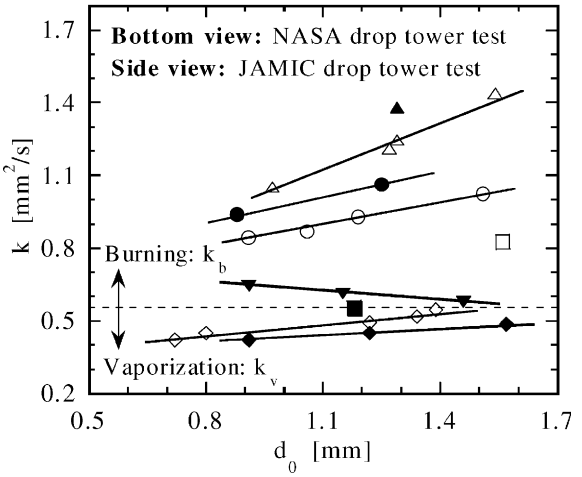

Fig. 4. Correlation of rate constant k with initial droplet diameter d_0 at different ambience temperatures.

Key	Reference	Fuel	d_0 [mm]
□	Jackson and Avedisian [7]	n-heptane	0.4-1.1
○		1-chloro-octane	0.4-1.1
△	Lee et al. [8]	n-heptane	0.8-1.8
▽	Marchese et al. [15]	n-heptane	1.0-3.5
◆	This work	n-decane	0.7-1.6

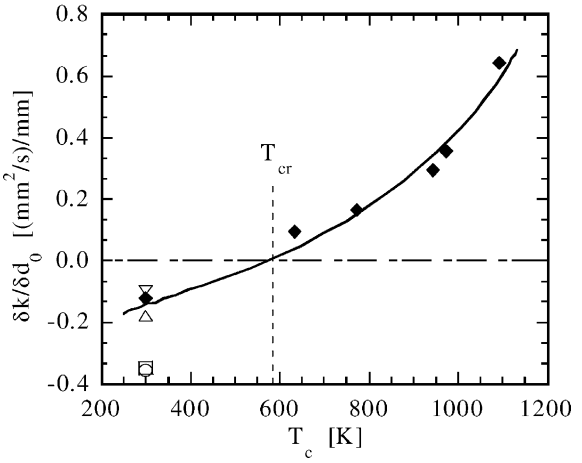

Fig. 5. Magnitude of initial diameter influence on droplet burning and vaporization rate constant varying with ambience temperature.

4. Evidence demonstration

Compared in Fig. 6 are the soot generations and accumulations of differently sized droplets at the same burning time relative to the initial droplet diameter squared, i.e. $(t - t_d)/d_0^2$, where $(t - t_d)$ was used to render the time starting from ignition. This offers also the first extension of the comparison to hot ambience, although a few similar reports were early made for the cold ambience burning [6,7]. As to each T_c compared, three different droplet sizes were selected (from NASA). Very like the burning in room temperature ambiences [6,7,11,17], soot precursors formed during burning and existed as a soot shell exclusively. At a given time $(t - t_d)/d_0^2$, the darkness of the image was generally higher for the initially larger droplet. Although the darkness difference appeared obscure early of burning (No. 1, a transient period), it become soon evident as the burning proceeded (after No. 2). Further, the local soot density at the soot shell was also higher for the initially larger droplet, especially lately during burning (after No. 2). All of these just comply with the room ambience burning. Thus, at a given time $(t - t_d)/d_0^2$ an initially larger droplet has definitely a higher local soot density at soot shell [8,17] and a greater total soot amount cross the fame [6–8], irrespective of the temperature of burning ambience.

Nevertheless, there are some particular characteristics of soot behaviors in hot ambience. An important one is the different soot generations at different T_c when compared against the same burning time for equi-sized droplets. As for $T_c = 943$ K and $T_c = 1093$ K in Fig. 6, it was revealed that the soot generation, represented by the soot amount inside the flame, is much less at the higher T_c [18]. This can be seen also from Fig. 6 by comparing the 1.19-mm (a) and 1.27-mm (b) droplets as well as the 0.92-mm (a) and 0.97-mm (b) droplets. At the similar time $(t - t_d)/d_0^2$, such as No. 2, even No. 3, the images in Fig. 6(a) have obviously higher darkness both at soot shell and cross the flame (Fig. 6(b) having longer time for No. 3), implying thus a higher soot generation at 943 K. Succeeding to this, Fig. 7 extends a comparison by including the cold ambience of the apparatus I (first inset). The other two tests in Fig. 7 are from the apparatus II at T_c equating to 773 K (second inset) and 973 K (third inset). One should note that the image

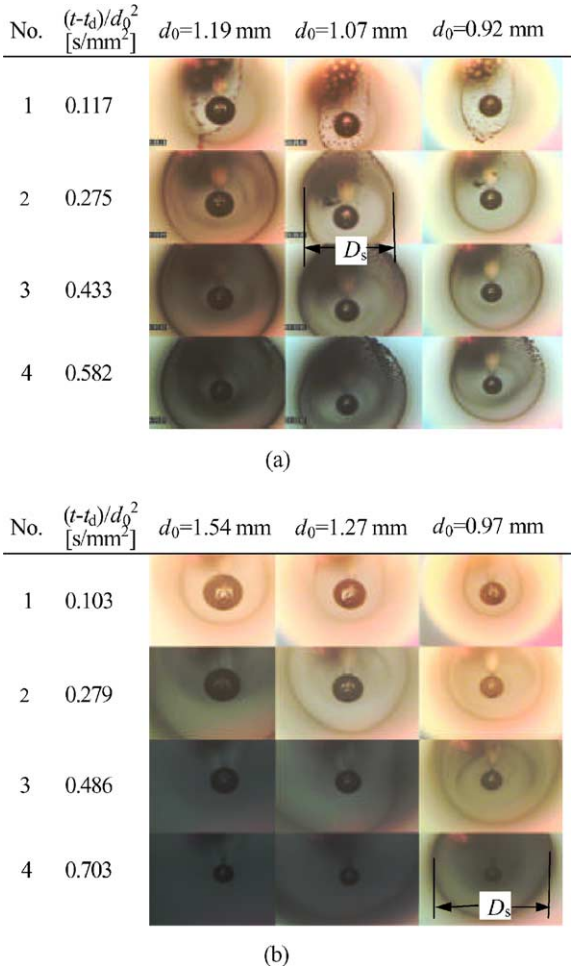

Fig. 6. Soot generation vs. relative burning time for droplets with different initial diameters (from NASA test). (a) $T_c = 943$ K, (b) $T_c = 1093$ K.

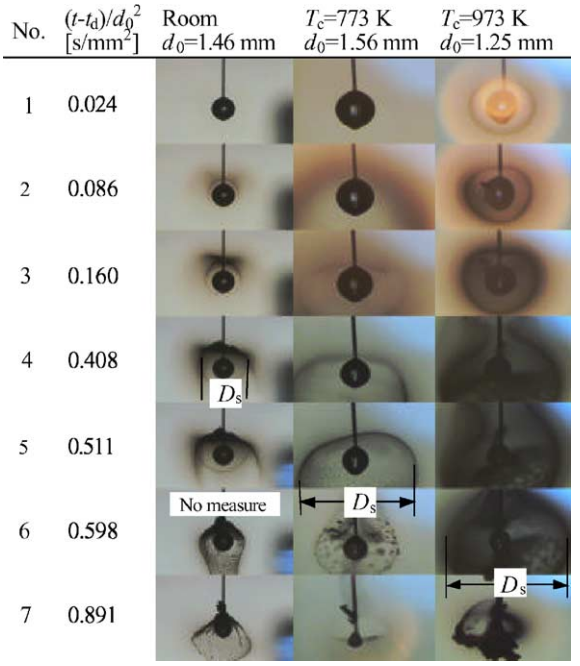

Fig. 7. Soot generation vs. relative burning time for droplets burnt at different ambience temperatures (from JAMIC test, the image magnifications for room and hot ambiences were different).

magnifications for apparatus I and II are different. Although the droplet at 773 K was biggest (2nd inset), its soot content at each compared instance appeared smallest. On the contrary, the smallest droplet at 973 K (third inset) possessed the highest soot generation that shows, for example, as the earliest formation of a soot shell (No. 1), highest local soot concentration at soot shell (Nos. 1–6), and greatest soot retainment within the flame (Nos. 1–7). The higher soot generation at room temperature (first inset) than at 773 K (second inset) can be similarly seen from a greater total soot amount cross the flame (Nos. 2–7) and an earlier formation of a soot shell (No. 2). With all of these we have then a map of soot generation that takes two peak values respectively at room temperature and at about 1000 K. The latter peak was also observed by Nakanishi et al. [33] through measuring the bulk soot generation of isolated fuel droplet burned in normal-gravity. It was suggested to be due to the quicker soot oxidation, than soot formation, that prevails at higher temperature. While this appears true and denotes a competition between the kinetic rates of soot formation and oxidation, the first peak at lower temperature would be more likely to correlate with the time-scale effect, as is interpreted below.

At lower temperatures, the Stefan flow that pushes the soot particles to the flame front is very smaller. This causes the soot precursors to move rapidly from flame front to flame interior and to stagnate nearby the droplet. On the other hand, the flame of usually tested droplets ($d_0 < 2.0$ mm) in room ambience would have still oxidation ability to the soot precursors. Thus, the very short time of staying in the flame front has to let the precursors mostly drift to the droplet vicinity and to accumulate there as a shell. This shows just the fact that a soot shell quickly formed closing the droplet in the first inset of Fig. 7 (No. 2). Increasing the ambience temperature enhances soot formation, oxidation and the Stefan flow simultaneously, but the dominant increase, or the parameter that takes the largest magnitude of increment, appears in the sequence of Stefan flow, soot formation and soot oxidation. This forms then three regimes, with the first regime for increasing the Stefan flow most quickly, which in turn works to increase the residence time of soot precursors in the flame and to

make the precursors closer the flame front. As a consequence, the explicit soot generation has to decrease with increasing T_c. Meanwhile, the soot shell size also rapidly increases during the process. In the second regime, the soot formation rate, i.e. the fuel pyrolysis rate, increases most quickly, making thus the higher soot generation for higher T_c. The final regime corresponds to the analysis of Nakanishi et al. [33], which reveals actually a dominance of soot oxidation.

However, we need more evidences for the first regime, although several literature studies [33,34] supported the other two regimes. On the other hand, the serious cooling effect of quartz fiber may contribute to the higher soot generation at room T_c as well. It should be the fact that the cooling facilitates soot coagulation and deposition onto the fiber (first inset), which in turn impresses us with an explicitly higher soot generation. In hot ambiences (second, third insets), the fiber filament gets a temperature that is at least equal to T_c, whereby having much weakened soot deposition and its induced action on soot generation (deposition being invisible to the bottom view in Fig. 6).

Compared in Fig. 8 are the luminous flame sizes D_f, the lateral width of the flame in fact, of differently sized droplets for the burning in room air. For the comparison we indeed wished the data in hot ambience but we had not enough drops for such a measurement before this paper. Notwithstanding, the image data in Fig. 6 impressed us that in the hot chamber an initially larger droplet exhibited a larger D_f at each specified $(t - t_d)/d_0^2$. This is actually very like the burning at room temperature shown in Fig. 8(a) and (b). The figure corroborated the early reports of Lee et al. [8] and Nayagam et al. [11] that the flame size D_f is larger for initially larger droplet at any specified burning time $(t - t_d)$ or $(t - t_d)/d_0^2$. Fig. 8(c) presents a new correlation between D_f and the instantaneous droplet diameter d, showing that at the same d the flame size is also larger for initially larger droplet. Nevertheless, there exists a period near flame extinction in which the different droplets possess the

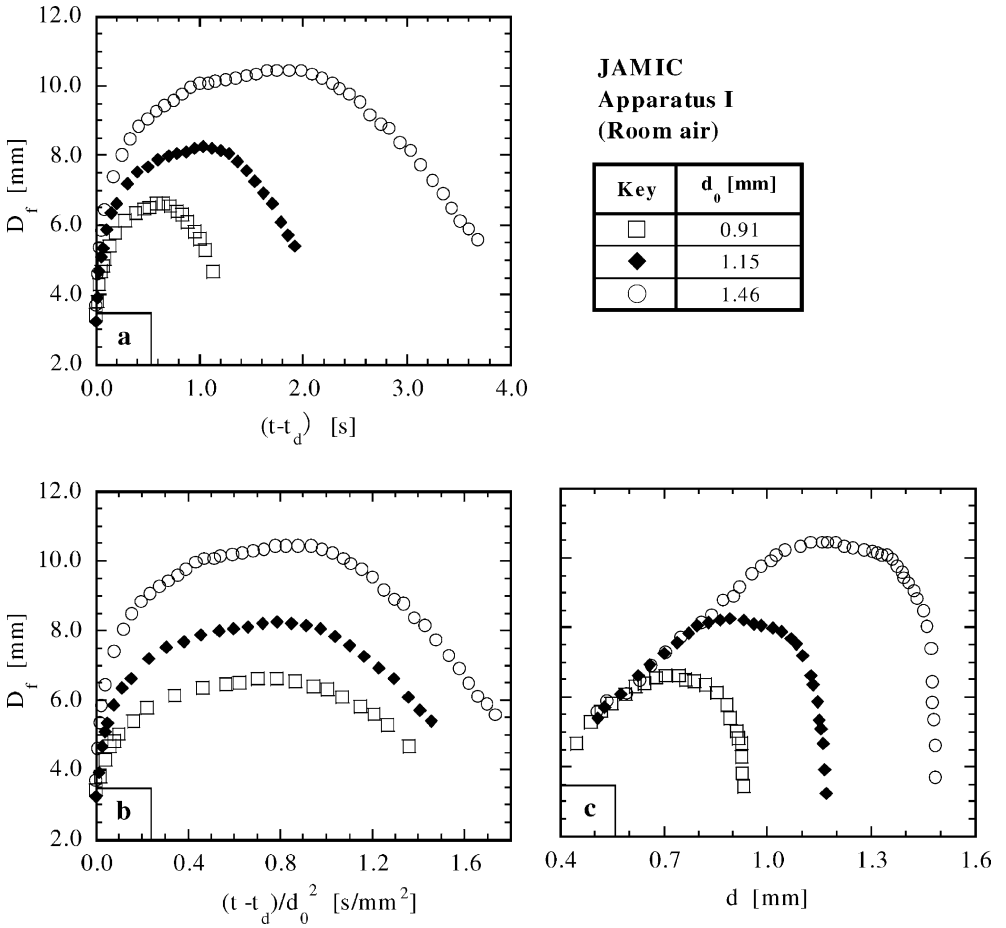

Fig. 8. Flame size variation during burning in room ambience for differently sized droplets (D_f refers to the lateral width of the flame).

same flame size. In this period the size D_f even tends to linearly correlate with the diameter d. Meanwhile, the whole lifetime of burning can be subdivided into three periods according to Fig. 8(c). Then, such a linear correlation of D_f with d may provide a good demarcation for the last period.

5. Result interpretation

In reasoning the initial diameter influence on droplet burning (vaporization) rate, we also accept that the thermal action of flame is dominant [8,16]. At the beginning of the article it was primarily indicated that the influence shows actually a flame-scale effect and is fully subject to the net heat defined in the article. The next will detail how the net heat forms via flame radiation and heat conduction and how it varies with the ambience temperature (convective heat being negligible in microgravity conditions).

Figs. 6 and 8 demonstrate that increasing the initial diameter d_0 increased the flame scale by leading to a higher soot amount inside the flame and a larger flame size at the same time $(t - t_d)/d_0^2$. Therefore, an initially larger droplet possesses surely a higher flame radiation, both non-luminously and luminously. The radiation works on droplet and ambience simultaneously. In ambiences with temperatures lower than, such as T_{cr} shown in Fig. 5, the latter (heat loss) would be excessively high and overwhelms the former. This causes then a negative net heat and makes the flame radiation to exhibit an overall effect of cooling the flame. When the radiation gets larger with increasing the flame size and soot amount, i.e. with raising the diameter d_0, the negative net heat becomes larger and consequently cools more the flame. This shown in burning rate forms just the decrease of the rate constant k with increasing d_0. As T_c increases, the heat loss by radiation decreases, while the heat gain to the droplet increases, under the controls of the increased flame temperature (but less than the increment in T_c) and little changed droplet temperature. It then diminishes the negative net heat gradually, and at a particular temperature (T_{cr}) reverses the net heat to a positive value. When this occurs, the increase in flame scale implies a higher heat input to the droplet, and as such the burning rate must get higher or larger d_0. Our tests in hot chamber rightly correspond to this case, showing essentially that in hot ambiences the flame radiation has an overall effect of enhancing the burning. From this view of point, the preceding analysis on the net heat is just consistent with a few other model predictions. While a number of calculations reported a cooling effect of flame radiation for room ambience [3–5,8,14–16], Chang and Shieh [35] identified an increase of burning rate by the flame radiation in a hot-air ambience of 1013 K.

Unlike radiation, the heat conduction does not proportionally vary with gas and soot mounts. It is subject more to the heat exchange surface and the temperature differential. The larger flame of a bigger droplet leads to a lower temperature gradient cross the flame, while it spreads the surface that conducts heat to the ambience. Both of these make then a greater heat loss to the ambience and a less heat gain to the droplet (neglecting the difference in conductivity for different d_0). Regardless of ambience temperature, those would surely reduce the burning rate as the flame gets larger with raising the diameter d_0. Compared to the experimental observations in Figs. 4 and 5, it shows consequently that the net heat via flame radiation is dominant over the initial diameter influence on the droplet burning rate, although the heat conduction might be significant in some cases (see [26]).

Fig. 5 clarifies that the initial diameter influence $(\delta k/\delta d_0)$ gradually increases with increasing T_c, which just corresponds to the gradual increase in the net heat. However, the soot generation with respect T_c exhibited two peak values in Figs. 6 and 7. Especially, at the tested higher T_c around 1100 K there was less soot generation than at about 973 K, but the influence in Fig. 5 considerably increased from 943 to 1093 K. This reveals that only luminous radiation cannot completely decide the effect of flame radiation [16]. In fact, even for less-sooting flame of *n*-heptane droplets, the burning rate similarly decreased with increasing d_0 in room air ambience [7,8,15]. Nonetheless, the luminous radiation may play an important role as well. The sooting fuel LCO was identified to have a larger initial diameter influence on burning rate than the less-sooting *n*-decane [31]. There existed different concerns about the relative importance of the two types of radiation. The luminous radiation was considered unimportant by [5], important by [35,36], important only to heat loss by [8], and important to flame wake but unimportant near wake by [37]. This work is unable to clarify such inconsistence, but feels that the relative importance depends on problem, especially on the analysis objective and burning conditions (fuel and temperature). When analyzing the net heat of sooting fuels, such as of LCO, both kinds of radiation should be accounted for.

The increasing degree of the initial diameter influence, $\delta(\delta k/\delta d_0)/\delta T_c$, is larger at higher T_c. It is surely owing to a rapid increase of the net heat with increasing T_c at higher temperature. The quicker increase of net heat at higher T_c may be related to many influential factors (unknown yet), but the temperature action on radiation would be dominant. That is, the radiation is subject to temperature by an index of four, the same change in T_c then must cause a larger decrease in the heat loss to the ambience if T_c is higher (case calculation can give this).

The rate of droplet vaporization (without burning) in the tested hot ambiences also increased with increasing

T_c, although the increasing magnitude $\delta k/\delta d_0$ was slighter. To this case the above analysis on the net heat via flame radiation should be similar applicable, if changing the flame radiation to the fuel vapor emission. Because the emissivity of fuel vapors, especially of alkane vapors, is lower than that of burning products (water vapor, carbon dioxide, soot, etc.), there show lower initial diameter influences for vaporization in Figs. 3–5. Nevertheless, this concern about the effect of fuel vapor emissivity warrants further examination. On the other hand, we should note that the heat conduction acts little on the initial diameter influence in the case of vaporization, especially when supposing the fuel vapor gets a temperature equating to T_c soon after its vaporization from the droplet.

In addition, we may wonder how the radiation from ambience, such as from oven wall, works with the net heat and the initial diameter influence. At the same transient droplet diameter d, such radiation would not lead to direct difference in drop heating and burning rate for initially differently sized droplets. Notwithstanding, a larger flame and a higher soot amount around the droplet (corresponding to an larger d_0) should absorb more of the radiation, which increases thus the flame temperature and enhances the flame radiation accordingly. This, in essence, clarifies that the ambience radiation can work on the net heat and the initial diameter influence only via the flame radiation. Hence, the preceding mechanism of net heat for determining the initial diameter influence would be generally valid irrespective of the existence of ambience radiation. In other words, the net heat denotes the heat balance between flame and ambience, which concerns already the action of ambience radiation.

6. More examination

The soot shell size is obviously measurable in Figs. 6 and 7. For room ambience burning there are several reports about the size [7,11,16,17], but very few data are available for hot ambience burning. Succeeding to Ref. [18], Fig. 9 intends to demonstrate further the difference in soot shell sizes between room and hot ambiences by comparing the data for both the cases. The measurements of the size are illustrated in Figs. 6 and 7, corresponding to various types of soot shells. In general, the size was determined as the largest internal width D_s of the shell. Applying to the bottom (Fig. 6) and side views (Fig. 7), that size represents the same horizontal aspect of the shell sphere, ensuring thus a consistence between the two data sources. Nonetheless, no measure was made after the igniter withdrawal for the burning in room air, on account of the serious shell deformation induced by the withdrawal. The selected data in Fig. 9 are for three different T_c (including room temperature), and at each T_c two different droplets are compared. For the larger droplets, only a period early of burning was measured since the shell exceeded the camera vision range in the succeeding burning (Fig. 6(b)).

Fig. 9(a) shows that the size D_s was larger for higher T_c at a given instantaneous droplet diameter d, making the room ambience burning had actually the smallest soot shell. This is consistent with the fact that at lower T_c there is a very weak Stefan flow around the droplet. Fig. 9(b) compares D_s against the relative burning time $(t-t_d)/d_0^2$, showing again that the droplets with similar initial diameters have bigger soot shell at higher T_c. Especially, one may note that the 1.45-mm droplet in room air (■) had yet smaller D_s than the 1.01-mm (●) and 0.95-mm (○) droplets in hot ambience. The increase of D_s with T_c should be mainly attributed to the corresponding increases in burning rate and Stefan flow. At the same T_c, Fig. 9(a) and (b) demonstrate that D_s also increased with increasing d_0. This is subject to the larger flame size at the same $(t-t_d)/d_0^2$ for the initially larger droplet (Fig. 8). A bigger flame reduces the temperature gradient inside the flame, which decreases the thermophoresis and in turn increases the soot shell size D_s. The different burning rates of differently sized droplets may influence the relationship between D_s and d_0 as well, but the action is weaker compared to the foregoing flame effect. For example, the lower burning rate of an initially larger droplet in room ambience would lead to a lower Stefan flow and consequently a smaller soot shell. This, however, is not the fact shown in Fig. 9(a) and (b) where D_s similarly increased with raising d_0 for cold and hot ambiences. Fig. 9(c) correlates D_s/d with $(t-t_d)/d_0^2$, indicating that the value of D_s/d was lower at lower T_c, especially lately of burning. A peak value of D_s/d manifested near the flame extinction, and Fig. 9(c) clarifies that this peak value was greater at higher T_c (more details being in [18]).

As a supplement to Fig. 8, Fig. 10 correlates the relative luminous flame size D_f/d with the times $(t-t_d)$ and $(t-t_d)/d_0^2$. As many other studies noted [7,8,21,23,38], the value D_f/d monotonically increased with burning, showing a violation of the classic quasi-steady theory [29,39]. Unlike D_f in Fig. 8(a), the value of D_f/d in Fig. 9(a) is larger for initially smaller droplets at specified $(t-t_d)$. It reveals a non-proportional scaling of the flame with droplet at the same $(t-t_d)$. That is, a double-sized droplet cannot make a flame twice larger when experiencing a given burning time. Fig. 10(b) is a similar plotting as in literature reports [7,8]. For *n*-heptane droplet, Jackson and Avedisian [7] suggested that the curves of D_f/d vs. $(t-t_d)/d_0^2$ be independent of d_0, implying the proportional scale-up of the flame size and burning time with d_0^2. Based on Fig. 10(b) we may say that this appears true, but more precisely we feel that D_f/d is yet slightly higher for smaller d_0 at the same $(t-t_d)/d_0^2$. Especially, Fig. 10(b) shows that with

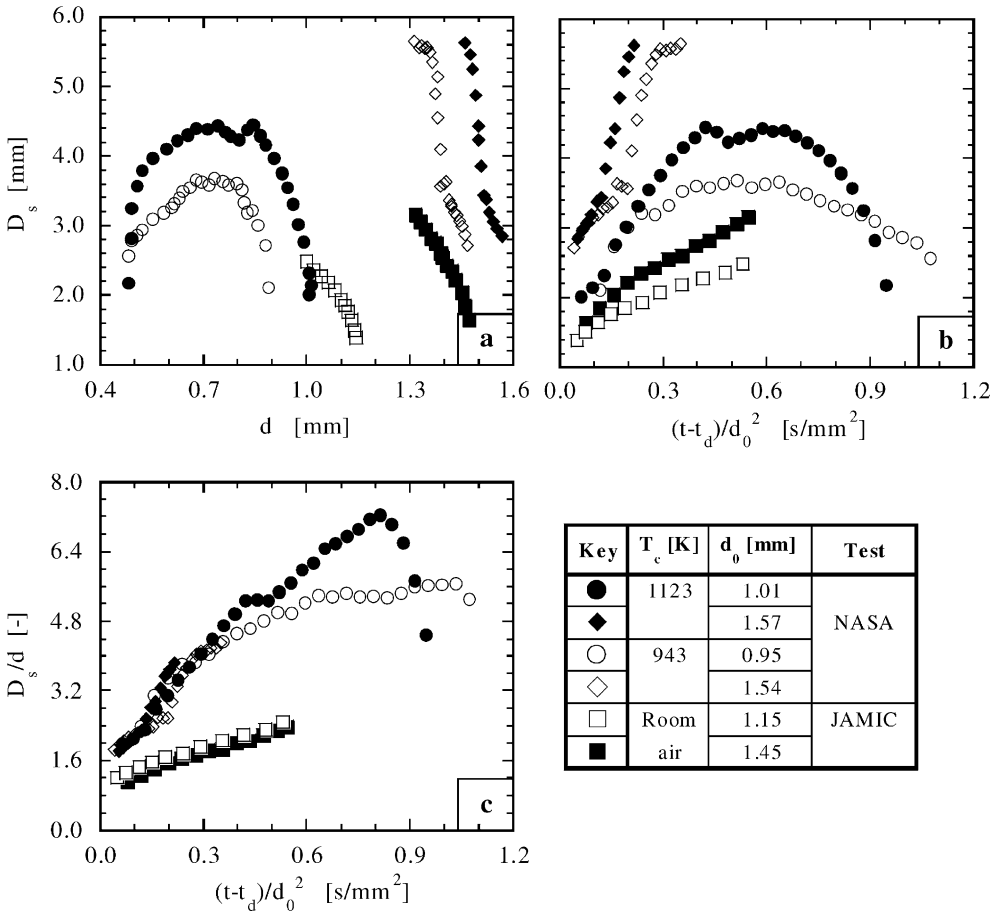

Fig. 9. Soot shell size variation during burning at different ambience temperatures for different droplets (D_s refers to the lateral width of the shell).

burning the difference among different droplets becomes gradually evident. Similar to Fig. 9(c) for D_s/d, Fig. 10 demonstrates a peak value for D_f/d near (almost at) the flame extinction. In room air, Manzello et al. [16] found that this maximal D_f/d slightly descended with ascending d_0. The data in Fig. 10 likely agree with such a statement, but the dependence is really weak for the presently tested d_0 (0.9–1.5 mm). Beyond all, we think that the ambience temperature may greatly vary the above results for D_f, as we had similarly observed for D_s [18]. Therefore, further examination on the flame size in hot ambience is valuable and highly wished.

Through adjusting the initial droplet diameter d_0, the work had realized an operation that vaporizes and burns the droplet at the same ambience temperature of $T_c = 773$ K (JAMIC). The ignition (for *n*-decane droplet) is slow at this T_c. The initially smaller droplets then may be unignited or ignited near the droplet depletion, allowing thus the determination of the droplet vaporization rate (k_v). On the other hand, the ignition of other larger droplets may occur at such instantaneous droplet sizes that enable the formation of a quasi-steady burning phase. In this case, the droplet burning rate (k_b) can be decided. Fig. 11 shows the virgin data of d^2 vs. t and the corresponding rate constant k for two droplets tested according to such a concern (k_b and k_v being also in Fig. 5). Although there might be experimental deviations, the major difference between the acquired k_b and k_v would show exclusively the contribution of flame heating to droplet gasification (here, ignoring the influence of d_0 on k). The ratio of k_v/k_b is just equal to the ratio of total heat transferred to the droplet in the cases of vaporization and burning. According to Fig. 11 we have $k_v/k_b = 0.668$. If treating the total heat for burning as 100%, such a k_v/k_b clarifies that the presence of a flame around the droplet provided a heat contribution of about 35%, including both heat conduction and flame radiation. Via model estimations, there were many judges on the percentage of flame radiation contribution, for instance, about 40% by [36], more than 50 % by [35], less than 20% by [1], less than 15% by [2], and only about 5% by [40]. The k_v/k_b shown here provides actually an

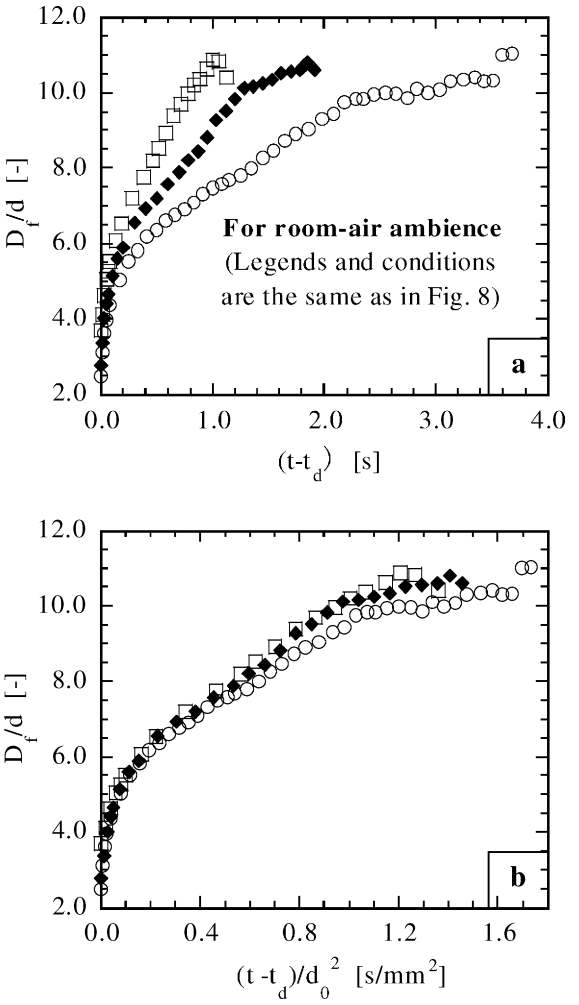

Fig. 10. Relative values of flame size to droplet diameter for different droplets in room ambience.

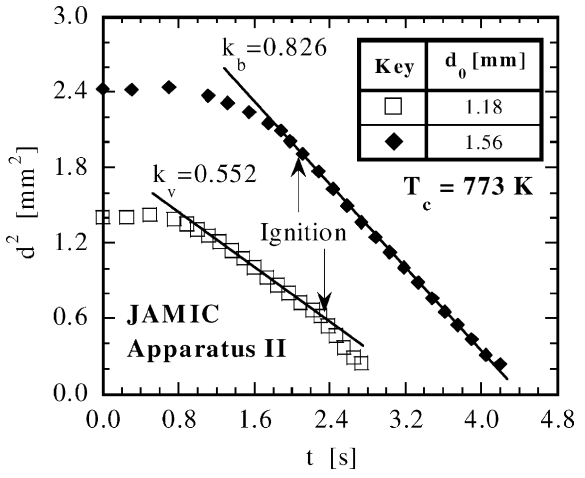

Fig. 11. Difference between vaporization (k_v) and burning (k_b) rates at a given ambience temperature—clarification of the heat amount transferred to droplet via flame.

evaluation for such judgments, that is, the contribution by the flame radiation alone must be less than 35% of the total heat consumed. Nonetheless, the measurement was only for $T_c = 773$ K, and further examination is needed to show how the ratio varies with T_c. Intuitionally, the percentage should decrease with increasing the ambience temperature, and at room T_c it is 100%.

7. Conclusions

(1) The influence of initial diameter on droplet burning rate was suggested to be a flame scale effect that is subject to the overall thermal action of flame in balance with ambience. This resulted in a definition of a net heat for the flame that denotes the difference between heat gain by the droplet and heat loss to the flame surrounding, and further enabled the analysis of the initial diameter influence in terms of the net heat for ambiences with different temperatures.

(2) In cold ambience (at room temperature), the excessive large heat loss caused a negative net heat, which decreased the burning rate of initially larger droplet. When the ambience temperature increased to lessen the heat loss in hot ambience, the net heat turned gradually positive and as a consequence led the larger droplet to exhibit a higher burning rate. The gradual reversion of the net heat from negative to positive produced a gradual reversion in the initial diameter influence, but the influence was larger at higher temperature. The latter just corresponds to the quicker increase of the net heat with raising the ambience temperature in such a case.

(3) Raising the initial droplet diameter increased the flame scale that shows as a bigger luminous flame and a higher soot generation (soot content in the flame) at a given burning time relative to the initial droplet diameter squared. These allowed the net heat from flame radiation, both luminous and non-luminous, to proportionally vary with the initial droplet diameter. Via heat conduction however, the heat loss to the ambience likely increases with increasing the flame scale, irrespective of ambience temperature. It derived that the flame radiation is dominant over the net heat and initial diameter influences clarified above.

(4) The ambience temperature greatly affected the soot generation during burning that was shown with the soot content cross the flame. Peak generations were identified at both the room temperature and a temperature of about 1000 K. The excessive lower Stefan flow and the kinetic competition between soot formation and oxidation were considered

responsible for such two peaks, respectively. Measurement of soot shell sizes revealed that the size was much smaller for the burning in room air, which, to some extent, verified the lower Stefan flow for cold ambience. Further, it was found that the increase in ambience temperature progressively increased the soot shell size, and the size increment appeared particularly obvious after an initial period of transient burning.

(5) By measuring the droplet vaporization and burning rates in a hot ambience of 773 K, the work showed quantitatively that the heat contribution of flame to the total heat consumed in fuel vaporization is hardly over 40% at this ambience temperature. The estimation included both heat conduction and flame radiation, implying that the flame radiation alone would take a rather smaller percentage under the tested conditions.

(6) Measuring the luminous flame size for the room ambience burning found that there exists a period before flame extinction where the flame sizes of differently sized droplets are correlated with the instantaneous droplet diameter by a single straight line. At the same burning time the initially larger droplet exhibited a greater flame size, but the standoff ratio of flame to droplet was inversely larger for smaller droplet.

Acknowledgements

The study was sponsored by the Japan Space Utilization Promotion Center (JSUP), and was financed by the New Energy and Industrial Technology Development Organization (NEDO).

References

[1] H.C. Hottel, G.C. Williams, H.C. Simpson, Combustion of droplets of heavy liquid fuels, 5th Symp. (Int.) on Combust., The Combustion Institute, Pittsburgh, 1955, pp. 101–129.

[2] J.A. Bolt, M.A. Saad, Combustion rates of freely falling fuel drops in a hot atmosphere, 5th Symp. (Int.) on Combust., The Combustion Institute, Pittsburgh, 1957, pp. 717–725.

[3] B.H. Chao, C.K. Law, J.S. T'ien, Structure and extinction of diffusion flames with flame radiation, 23rd Symp. (Int.) on Combust., The Combustion Institute, Pittsburgh, 1990, pp. 523–531.

[4] J. Buckmaster, G. Joulin, P. Ronney, The structure and stability of nonadiabatic flame balls, Combust. Flame 79 (1990) 381–392.

[5] T. Saitoh, K. Yamazaki, R. Viskanta, Effect of thermal radiation on transient combustion of a fuel droplet, J. Thermophys. Heat Transfer 7 (1993) 94–100.

[6] G.S. Jackson, C.T. Avedisian, J.C. Yang, Observations of soot during droplet combustion at low gravity: heptane and heptane/monochloroalkane mixtures, Int. J. Heat Mass Transfer 35 (1992) 2017–2033.

[7] G.S. Jackson, C.T. Avedisian, The effect of initial diameter in spherically symmetric droplet combustion of sooting fuels, Proc. R. Soc. Lond. A 446 (1994) 255–276.

[8] K.-O. Lee, S.L. Manzello, M.Y. Choi, The effects of initial diameter on sooting and burning behavior of isolated droplets under microgravity conditions, Combust. Sci. Technol. 132 (1998) 139–156.

[9] C.T. Avedisian, J.H. Bae, Combustion of sooting mixture droplets at low gravity, 6th Int. Microgravity Combust. Workshop, NASA GRC, Cleveland, 2001, pp. 249–252.

[10] A.J. Marchese, F.L. Dryer, R.O. Colantonio, Radiative effects in space-based methanol/water droplet combustion experiments, 27th Symp. (Int.) on Combust., The Combustion Institute, Pittsburgh, 1998, pp. 2627–2634.

[11] V. Nayagam, J.B. Haggard Jr., R.O. Colantonio, A.J. Marchese, F.L. Dryer, B.L. Zhang, F.A. Williams, Microgravity *n*-heptane droplet combustion in oxygen–helium mixtures at atmospheric pressure, AIAA J. 36 (1998) 1369–1378.

[12] F.A. Williams, Experiments on droplet combustion in spacelab and space station: planning, data analysis and theoretical interpretations of results, 6th Int. Microgravity Combust. Workshop, NASA GRC, Cleveland, 2001, pp. 229–232.

[13] F.L. Dryer, A. Kazakov, B.D. Urban, Some recent observations on the burning of isolated *n*-heptane and alcohol droplets, 6th Int. Microgravity Combust. Workshop, NASA GRC, Cleveland, 2001, pp. 233–236.

[14] A.J. Marchese, F.L. Dryer, The effect of non-luminous thermal radiation in microgravity droplet combustion, Combust. Sci. Technol. 124 (1997) 371–402.

[15] A.J. Marchese, F.L. Dryer, V. Nayagam, Numerical modeling of isolated *n*-alkane droplet flames: initial comparisons with ground and space-bases microgravity experiments, Combust. Flame 116 (1999) 432–459.

[16] S.L. Manzello, M.Y. Choi, A. Kazakov, F.L. Dryer, R. Dobash, T. Hirano, The burning of large *n*-heptane droplets in microgravity, 28th Symp. (Int.) on Combust., The Combustion Institute, Pittsburgh, 2000, pp. 1079–1086.

[17] M.Y. Choi, K.-O. Lee, Investigation of sooting in microgravity droplet combustion, 26th Symp. (Int.) on Combust., The Combustion Institute, Pittsburgh, 1996, pp. 1243–1249.

[18] G. Xu, M. Ikegami, S. Honma, K. Ikeda, H. Nagaishi, D.L. Dietrich, P.M. Struk, Soot formation from isolated liquid fuel droplet burning in a microgravity hot chamber, AIAA J., submitted for publication.

[19] S. Kumagai, T. Sakai, S. Okajima, Combustion of free fuel droplets in a freely falling chamber, 15th Symp. (Int.) on Combust., The Combustion Institute, Pittsburgh, 1975, pp. 779–785.

[20] S. Okajima, S. Kumagai, Further investigations of combustion of free droplets in a freely falling chamber including moving droplets, 15th Symp. (Int.) on Combust., The Combustion Institute, Pittsburgh, 1975, pp. 401–407.

[21] H. Hara, S. Kumagai, Experimental investigation of free droplet combustion under microgravity, 23rd Symp. (Int.) on Combust., The Combustion Institute, Pittsburgh, 1990, pp. 1605–1610.
[22] M.Y. Choi, F.L. Dryer, J.B. Haggard Jr., Observations on a slow burning regime for hydrocarbon droplets: *n*-heptane/air results, 23rd Symp. (Int.) on Combust., The Combustion Institute, Pittsburgh, 1990, pp. 1597–1605.
[23] H. Hara, S. Kumagai, The effect of initial diameter on free droplet combustion with spherical flame, 25th Symp. (Int.) on Combust., The Combustion Institute, Pittsburgh, 1994, pp. 423–430.
[24] T. Suekane, K. Yasutomi, S. Hirai, Study on combustion behavior of single droplet in free fall generated by using ultrasonic levitation technique, 38th Symp. (Japan) on Combust., The Combustion Society of Japan, Tokyo, 2000, pp. 191–192.
[25] D.L. Dietrich, J.B. Haggard Jr., F.L. Dryer, V. Nayagam, B.D. Shaw, F.A. Williams, Droplet combustion experiments in spacelab, 26th Symp. (Int.) on Combust., The Combustion Institute, Pittsburgh, 1996, pp. 1201–1207.
[26] S.Y. Cho, M.Y. Choi, F.L. Dryer, Extinction of a free methanol droplet in microgravity, 23rd Symp. (Int.) on Combust., The Combustion Institute, Pittsburgh, 1990, pp. 1611–1617.
[27] B.L. Zhang, F.A. Williams, Effects of the Lewis number of water vapor on the combustion and extinction of methanol drops, Combust. Flame 112 (1998) 113–120.
[28] G.M. Faeth, D.R. Olson, The ignition of hydrocarbon fuel droplets in air, SAE Trans. 76, Paper 680465, 1968, pp. 1793–1802.
[29] G.A.E. Godsave, Studies of the combustion of drops in a fuel spray—the burning of single drops of fuel, 4th Symp. (Int.) on Combust., The Combustion Institute, Pittsburgh, 1953, pp. 818–830.
[30] G. Xu, M. Ikegami, S. Honma, K. Ikeda, H. Nagaishi, D.L. Dietrich, Y. Takeshita, Burning droplets composed of light cycle oil and diesel light oil, Energy Fuels 16 (2002) 366–378.
[31] G. Xu, M. Ikegami, S. Honma, M. Sasaki, K. Ikeda, H. Nagaishi, Y. Takeshita, Combustion characteristics of droplets composed of diesel light oil and light cycle oil in a hot chamber, Fuel 82 (2003) 319–330.
[32] M.T. Monaghan, G. Siddall, M.W. Thring, The influence of initial diameter on the combustion of single drops of liquid fuel, Combust. Flame 12 (1968) 45–53.
[33] K. Nakanishi, T. Kadota, H. Hiroyasu, Effect of air velocity and temperature on the soot formation by combustion of a fuel droplet, Combust. Flame 40 (1981) 247–262.
[34] I. Glassman, Soot formation in combustion processes, 22nd Symp. (Int.) on Combust, The Combustion Institute, Pittsburgh, 1988, pp. 295–311.
[35] K.-C. Chang, J.-S. Shieh, Theoretical investigation of transient droplet combustion by considering flame radiation, Int. J. Heat Mass Transfer 38 (1995) 2611–2621.
[36] S.I. Abdel-Khalik, T. Tamaru, M.M. El-wakil, A chromatographic and interferometric study of the diffusion flame around a simulated fuel drop, 15th Symp. (Int.) on Combust., The Combustion Institute, Pittsburgh, 1975, pp. 389–399.
[37] S.R. Gollahalli, T.A. Brzustowski, Experimental studies on the flame structure in the wake of a burning droplet, 14th Symp. (Int.) on Combust., The Combustion Institute, Pittsburgh, 1973, pp. 1333–1344.
[38] M.K. King, An unsteady-state analysis of porous sphere and droplet fuel combustion under microgravity conditions, 26th Symp. (Int.) on Combust., The Combustion Institute, Pittsburgh, 1996, pp. 1227–1234.
[39] D.B. Spalding, The combustion of liquid fuels, 4th Symp. (Int.) on Combust., The Combustion Institute, Pittsburgh, 1953, pp. 847–864.
[40] P.L. Lage, R.H. Rangel, Single droplet vaporization including thermal radiation absorption, J. Thermophys. Heat Transfer 7 (1993) 502–509.